# *Chapter-2*

## *Experimental details*

## 2.1 Introduction

This chapter is dedicated to describe the experimental techniques and procedures that were adopted to prepare the samples and characterization techniques that were involved to characterize and describe the properties of the prepared samples. In this thesis, Mo-substituted $PbTiO_3$ and Mn-substituted $BiYO_3$ powder samples are prepared by solid state reaction method. The Mo-substituted $PbTiO_3$ is prepared by both the low energy ball milling process and high energy ball milling process while later compounds like $BiY_{(1-x)}Mn_xO_3$ and $(Bi_{0.5}Li_{0.5})_xBa_{(1-x)}TiO_3$ were prepared by high energy ball milling process in solid-state powder method. Such prepared samples were calcined at different temperatures and optimization of calcination temperature was done. These calcined powders were used for characterizations like x-ray diffraction phase analysis, TGA-DSC thermal analysis, Optical analysis, morphological analysis etc. Powder samples cannot be used for some characterisations where we need two terminals to apply electrical signal like Complex Impedance analysis, dielectric measurements, Ferroelectric analysis etc. Therefore, dense pellet preparation is required which is obtained by closed air sintering udder optimum conditions. After preparation, all the samples were subjected to different characterizations to evaluate their structural and physical properties. In the forthcoming sections, the important sample preparation and characterization steps are briefly described.

## 2.2. Sample Synthesis

Preparation of crystalline powder samples are done mainly by the following three methods. We have used the solid state method for preparation of our samples.

1. Solid state method
2. Sol gel method
3. Combustion method

### 2.2.1 Solid state reaction method

Solid state reaction method or powder method is one of the most widely used synthesis method for the preparation of polycrystalline ceramics and for the commercial production of the technologically important ceramics. This is a facile method uses easily available simple and economical oxides, hydroxides, oxalates, carbonates, nitrates, alkoxides, and easily available salts as the reactants. This method needs a simple and relatively low cost apparatus which are easy to process. Moreover, large amount production of powder can be done in a relatively simple manner [113, 114]. A homogeneous mixture of reactant powder particles is prepared through high-speed collision from the balls inside the high-speed rotating container and so named as ball milling. Usually, this process only gives homogeneous mixture and reaction take place at high temperature not at room temperature. Therefore, it is always followed by a heating process in order to occur reaction at a significant rate. Thermal and kinetic factors both play important role in the solid state reactions. When the speed of ball milling is quite high, the mechanical alloying can be done in some cases just without calcination. The different machine used are specifically attrition, horizontal ball mill, or a planetary ball mill. In this high energy ball milling method, balls used are of same material as that of containers, and are rotated and vibrated at predefined speed and duration. Zirconium dioxide (ZnO), Stainless Steel, Tungsten Carbide etc. is the commonly used materials for ball and container furnishing.

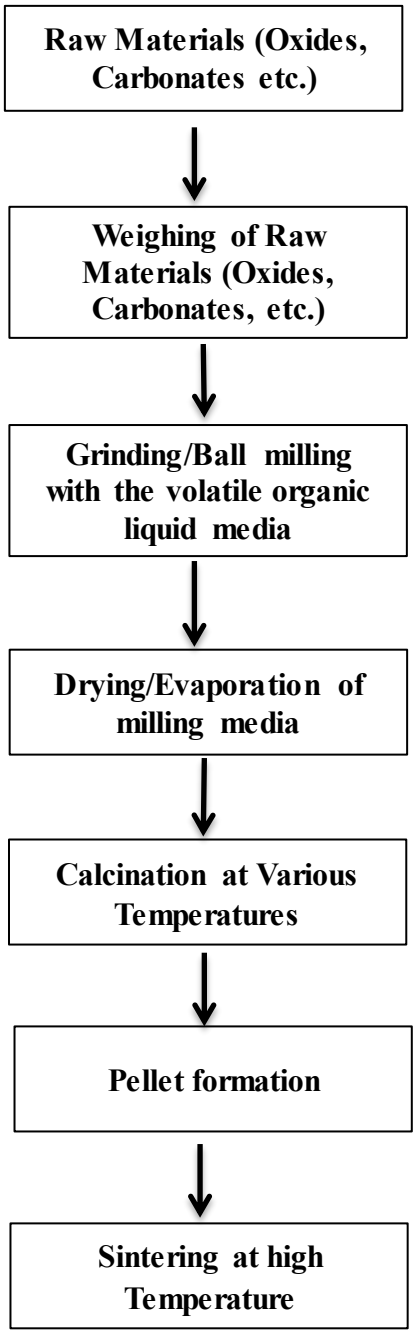


**Figure 2.1:** Flow chart of various steps involved in the solid state synthesis method.

The high energy ball milling synthesis technique has easy controlling parameters which control phase transformation conditions by energizing and dissociation condition of the starting raw materials. New phases and compounds may form after the raw materials get mixed, cold welded, fractured, dissociated and energized during

mechanical alloying. If not, a subsequent heat treatment at higher temperature, named as calcination process, may be required, for thermochemical reaction to take place for formation of product phase. As a final milled product, a mixture of nano powders is formed, then milling media (ethanol or acetone) is evaporated, subsequently the dried samples are grounded in agate mortar followed by calcination at various temperatures. Flow chart of steps involved in the solid-state method is shown in **Fig. 2.1**.

Some advantages of high energy ball milling are following: (i) Low-cost installation, facile, one step mechanochemical synthesis in some cases, (ii) User defined revolutions per minute (rpm) and sample milling time, (iii) Low-cost milling media, (iv) Appropriate for materials having all degrees of hardness, (v) Size of the final product is controllable, (vi) Nano sized sample can be formed.

### 2.2.2 Chemicals used for sample preparation

We have used oxides, carbonates and acetates for the preparation of our samples which are listed below

**Table 2.1:** List of the raw materials used for preparation of different samples.

| **Compound Name** | **Raw Materials** | **Assay** |
|---|---|---|
| $Pb(Mo_xTi_{1-x})O_3$ ($x$ = 0.025, 0.05, 0.075, 0.10) | PbO (Hi-media)<br>$TiO_2$ (Sigma Aldrich)<br>$MoO_2$ (Sigma Aldrich) | 98%<br>99%<br>99% |
| $BiY_{(1-x)}Mn_xO_3$ ($x$ = 0.0, 0.10, 0.25, 0.50, 0.75) | $Bi_2O_3$ (Hi-media)<br>$Y_2O_3$ (Sigma Aldrich)<br>$Mn(CH3COO)_2.4H_2O$ (Sigma Aldrich) | 99%<br>99.99%<br>99% |
| $(Bi_{0.5}Li_{0.5})_xBa_{(1-x)}TiO_3$ ( $x$ = 0.10, 0.12, 0.15, 0.20, 0.25) | $BaCO_3$ (Hi-media)<br>$LiCO_3$ (Sigma Aldrich)<br>$Bi_2O_3$ (Hi-media)<br>$TiO_2$ (Hi-media) | 99%<br>99.99%<br>99%<br>99.5% |

## 2.3 Characterization Techniques

Different characterizations like x-ray diffraction (XRD), scanning electron microscopy (SEM), x-ray photoelectron spectroscopy (XPS), Impedance Spectroscopy and polarization (P)-Electric field (E) hysteresis loop analysis of various samples are done to study the various physical properties like structural, optical, dielectric, electrical and ferroelectric properties.

### 2.3.1 X-ray Diffraction

The most basic characterization, used to determine the crystalline nature and phase formation of materials is x-ray diffraction. By X-ray diffraction technique, chemical, physical and structural information about material can be investigated. The method is non-destructive and works by irradiating a material with X-rays. It reveals all crystallographic phases present in the polycrystalline powder and many crucial information about each crystallographic phase e.g. it's crystal structure or structural deviation from ideal structure, crystallite size, preferential ordering and epitaxial growth of crystallites can be precisely estimated. Crystals are regular array of atoms and they are ordered in such a way that they form a layer of parallel planes. The distance between each layer, known as interplanar separation 'd' is the characteristic property of the material. X-rays are high energy electromagnetic radiations, when x-ray falls on a crystal it interacts with the electron cloud of the atom and x-rays are scattered in all directions working as the source of spherical wave. A regular array of scattering sources (atoms) generates a regular array of spherical waves. These waves destruct each other in all directions except some specific directions specified by the Bragg's Law. As a result, the incident x-rays appear to be reflected from the plane of the crystal as shown in the Figure 2.3. The X-rays diffracted from atomic planes depend on length scale of periodic crystalline order and nature and relative position of atoms (in a motif). Typically, x-ray

radiation, generated from copper source with characteristic wavelength ($Cuk_{\alpha 1}$) ($\lambda$) =1.5406 Å are used for irradiation. Initially the produced x-ray are collimated then the collimated beams are made incident along all possible incidence angles θ, onto the sample and scattered x-ray is recorded with the help of detector. According to Bragg's Law, only those incident rays are reinforced after diffraction from the crystal which satisfies the Bragg's Law and these diffracted rays are recorded by the detector.

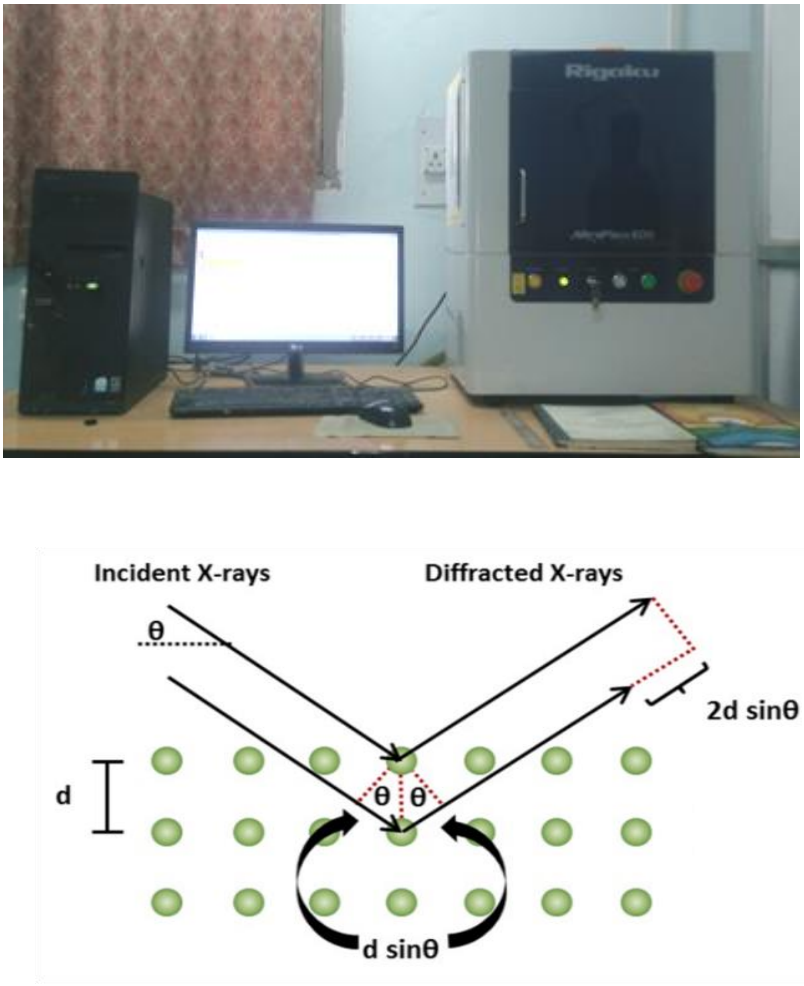


**Figure 2.2:** Schematic diagram showing the X-ray diffraction from a crystal lattice plane of a material [Barcikowski et al., 2016].

### 2.3.1.1 Bragg's Law

W. H. Bragg and his son W. L. Bragg explained X-ray diffraction phenomena using an relation among incident angles (θ), the wavelength of the incident x-ray beam (λ) and interplanar separation distance (d) known as Bragg's Law which is given as-

$$2dsin\theta = n\lambda \quad (2.1)$$

where n is an integer. x-ray diffraction is an example of x-ray wave interference where the scattered x-ray waves from regularly arranged atoms are interfering with each other resulting in a diffraction pattern as shown in **Fig. 2.2** [Barcikowski et al., 2016]. The diffraction phenomena of x-rays incident on the crystalline material are a direct evidence of parallel plane structure of crystals.

In case of XRD characterization of polycrystalline materials, Bragg's Law conditions are satisfied via changing angle (θ) because abundance of random oriented crystallites makes different inter planer spacing (d) available at every angle. In case of polycrystalline material, probability theory for large number reveals that almost equal number of crystallites will be there with a particular orientation. The characteristic diffractogram of particular sample is obtained by plotting intensities of diffracted wave and angular position of the X-rays. Diffractogram of a polycrystalline material with multiple phases is obtained as the superposition of individual patterns.

Rigaku MiniFlex X-ray diffractometer having Cu-$K_{\alpha 1}$ radiation of wavelength λ = 1.5406 Å with applied voltage rating 40 kV and current of 15 mA. The Si-powder was used as standard material to obtain the accurate value of 2θ for determination of the lattice parameters. Finely grounded and sintered polycrystalline materials were analysed by the XRD analysis in the scan range of 10º – 100º with scan rate of 1 degree/min and step size of 0.02º. The XRD pattern can also provide the average crystallite sizes of powder sample with the help of Scherrer's equation [115, 116]

$$D = \frac{K\lambda}{\beta \cos\theta} \tag{2.2}$$

where $K, \theta, \lambda$ are the shape factor (= 0.90), Bragg angle and wavelength of X-rays respectively and $\beta$ is the full width at half maxima [117] of the most intense Bragg peak in the XRD pattern. [117]

**2.3.1.2 Rietveld Refinement**

This is a structure refinement technique using powder diffraction data which helps to determine the many aspects of crystal structure. This method can directly estimate the unit cell structural parameters with the help of diffraction pattern. International Union of Crystallography (IUCr) illustrated the Rietveld structural refinement method as "***Technique of analysing X-ray powder diffraction data from which crystallographic structural information is obtained via refining the complete profile of the observed diffraction pattern until it complete matches with calculated profile using a least-squares approach"*** [118]. The first step of the whole process of Rietveld Refinement is to identify the crystalline phase(s) of the experimental powder XRD pattern with the help of search-match using standard database or trial-error method. After determination of the phase(s), if the material is already known, Crystallographic Information (CIF) File containing the detailed crystal structure is searched out from ICSD (Inorganic Crystal Structure Database) or COD (Crystallographic Open Database) database. If material is unknown, one needs to postulate a good starting structural model and proceed with the Rietveld structure refinement to verify that the considered structure is correctly modelling the experimental diffraction pattern. Some additional information are also necessary to be provided to proceed for structural refinement: (i) instrumental correction factors (instrumental peak shift, peak broadening and peak asymmetry) for the XRD pattern

calibration (ii) approximate values of crystallite size and lattice strain. A Rietveld structure refinement software, such as FullProf Suite, is used to simulate theoretical XRD pattern with the help of these preliminary information and CIF files. During refinement, instrumental correction parameters are kept fixed, and structural followed by microstructural parameters are successively refined via iterative mode until all the parameters are converged. The successive refinements of structural and microstructural parameters and instrumental correction parameters, leads to the "best fit" pattern where the difference between the calculated and experimental XRD pattern is negligible.

**2.3.1.3 The Rietveld Structure Refinement Software**

The structural refinement process from x-ray diffraction pattern is a complex process which deals with many calculations containing various parameters. There are various softwares being used globally for Rietveld structure refinement. In this thesis work, FullProf suit is employed for Rietveld refinement analysis. FullProf Suit have user friendly interface which shows the correlation of experimental and calculated pattern at each step. This software is proficient in the precise determination of structural parameters and microstructural parameters.

**Advantage of this software -**

(i) Crystal structure and microstructure refinement.

(ii) Simultaneously multiple phase quantitative analysis,

(iii) Automatic parameter modification for structure refinement.

(iv) XRD pattern of various type of powder, pellets or thin films can be refined.

(v) Defect and texture models Analysis.

(v) User friendly Interface.

### 2.3.2 Scanning Electron Microscopy (SEM)

Scanning electron microscopy (SEM) is a technique for high resolution surface imaging which can precisely measure the features of micro to nano scale objects. In this technique, beam of electrons (electron wave) is used for imaging just as visible light is used in light microscopy. SEM can have very high magnification upto 100,000 kX and high depth of field. In this microscopy, scanning through raster pattern by beam of electrons, generates high resolution images of the sample. **Fig. 2.3** shows the typical set-up of a modern scanning electron microscope. The schematic diagram of the apparatus illustrating the imaging mechanism is shown in **Fig. 2.4**. The key components of the Scanning Electron Microscope are electron source, magnetic lenses, scanning coil, sample chamber and detectors. The mounting of the samples is done on stubs using carbon tapes. The electron gun produces flood of electrons which is accelerated from 100 eV to 40 keV of energy. The beam travels throughout the vertical cavity in the microscope under high vacuumed conditions. The stream is focused by magnetic lenses into a 0.4 to 5 nm narrow beam and can be deflected in X-or Y direction by scanning coils and scans the sample surface in raster fashion. When this beam falls on the surface of sample, multiple events happen depending on the penetration depth of the sample as shown in **Fig. 2.5**. As a result of interaction, characteristic X-rays, backscattered electrons and secondary electrons come out from sample surface which are collected by the respective detectors and converted into the image signal that can be visualised on a computer screen. These signals are then interpreted to derive the information about sample's morphology, topography, defects and the distribution of elements.


**Figure 2.3:** Image of Scanning electron microscope ZEISS SUPRA 40.

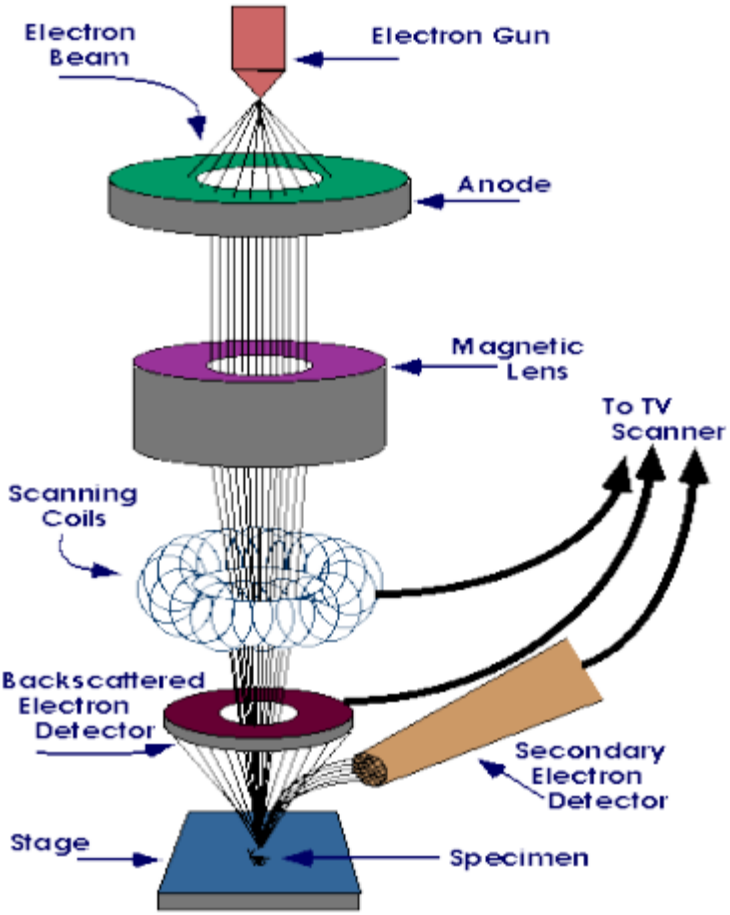


**Figure 2.4:** Schematic diagram showing the imaging mechanism of SEM [119].

In low conductive materials, charge can build up over the surface in static electric field. Charge build-up results in the static electric field and deflects the

secondary electron which creates difficulty in imaging. To avoid such charge build-up, the thin Au-coating by sputtering were applied to all samples. In this thesis, ZEISS EVO 18 and SUPRA 40 were used for SEM imaging of the sintered pellets. This instrument is proficient in taking high resolution images with excellent contrast at ultra-low (200V) and high (30kV) accelerating voltages and at high magnification range 50K ~100K. This electron microscope uses Lanthanum hexa boride ($LaB_6$) solid state single crystals as the source of electron beam. Measuring energy of emitted characteristic x-rays of the sample by x-ray detectors, known as energy dispersive spectroscopy is used to characterize the qualitative and quantitative presence of elements in the sample. Spatial distribution of elements can be determined through the elemental mapping of the sample by EDS.

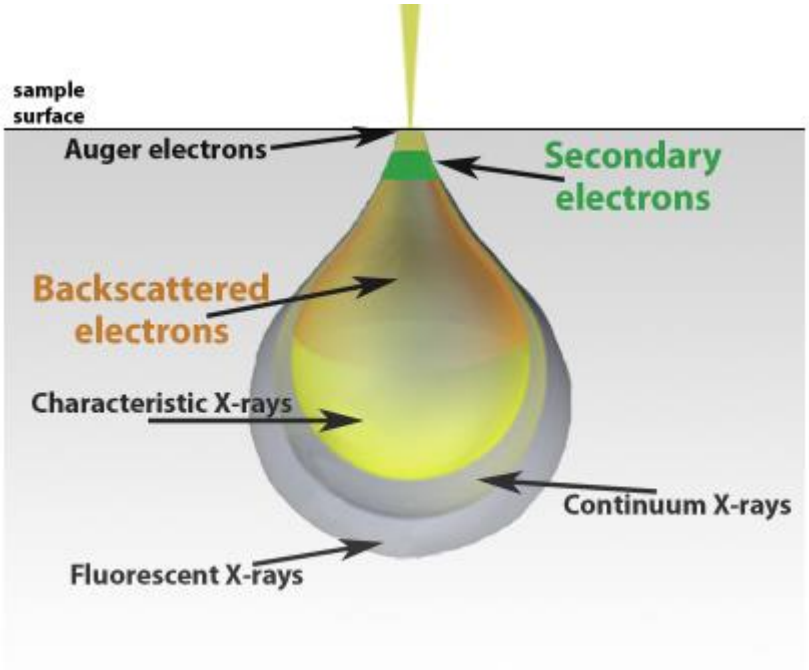


**Figure 2.5:** Schematic diagram showing the interaction of electron beam to the surface [120].

### 2.3.3 Thermal characterization technique: TGA-DTA

Thermo-gravimetric analysis-differential thermal analysis (TGA-DTA) characterizations give information about the thermal stability, physical and chemical change in the as synthesized sample, as a function of temperature. This technique measures the mass of the sample and change in heat/temperature simultaneously as a function of time or temperature when the sample is subjected to controlled and programmed heating. This is one of the fundamental techniques that gives information about calcination temperature of uncalcined mixture of raw materials, phase formation, phase transition temperature, reduction or oxidation temperature, solid state reaction temperature, absorption, desorption etc. [51].

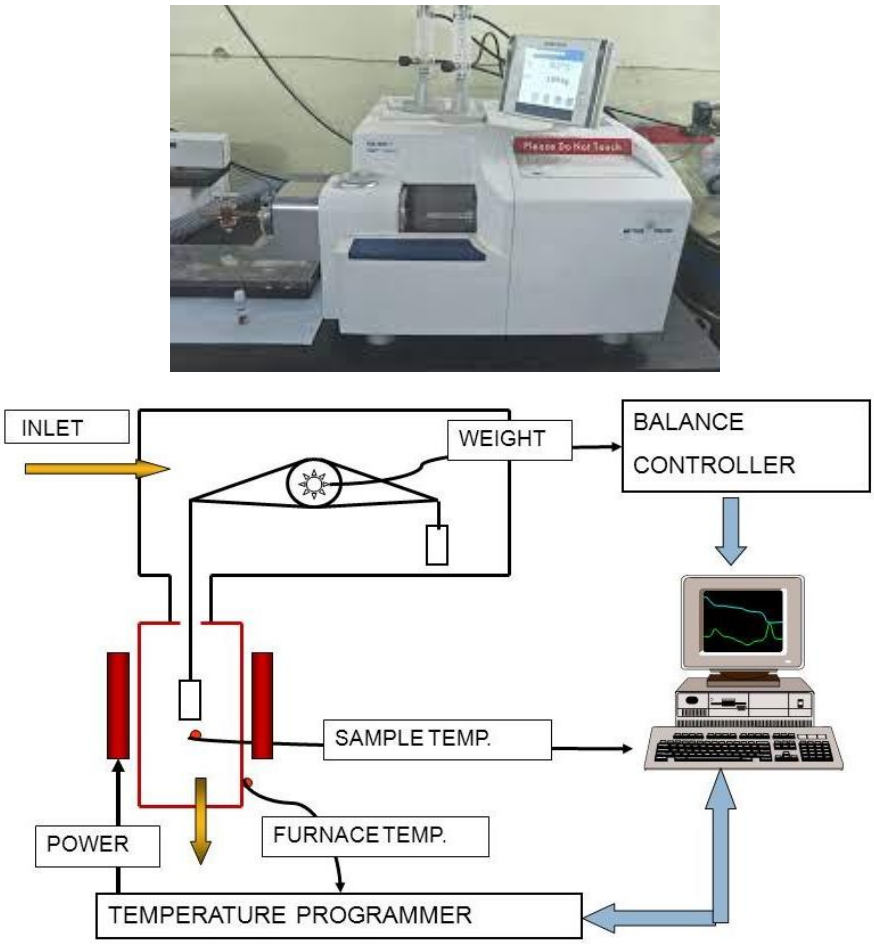


**Figure 2.6:** Schematic diagram TGA-DTA analyser (Mettler Toledo) set up. [121]

Moreover, TGA is extensively used to know degradation temperature and melting temperature of materials. **Fig. 2.6** shows the apparatus and the schematic diagram of instrumentation of the TGA-DTA analyser. There are two crucibles one for the sample and other for reference material to measure the heat/temperature difference between them. In this thesis, Mettler-Toledo TGA was used for thermal characterization of pre-calcined reactant mixture to determine the calcination temperature of the samples.

### 2.3.4 X-ray Photoelectron Spectroscopy (XPS)

X-ray photoelectron spectroscopy (XPS) can examine the presence of elements, their oxidation states, ratio of different oxidation state of an element and oxygen vacancies present in the sample. In this thesis, Thermo Fisher Scientific (K-alpha) XPS set up is used as shown in **Fig. 2.7** and XPSPEAK41 peak fitting software is employed for fitting and resolving the binding energy peaks. The **Fig. 2.7** also shows the outline of the working principle for XPS.

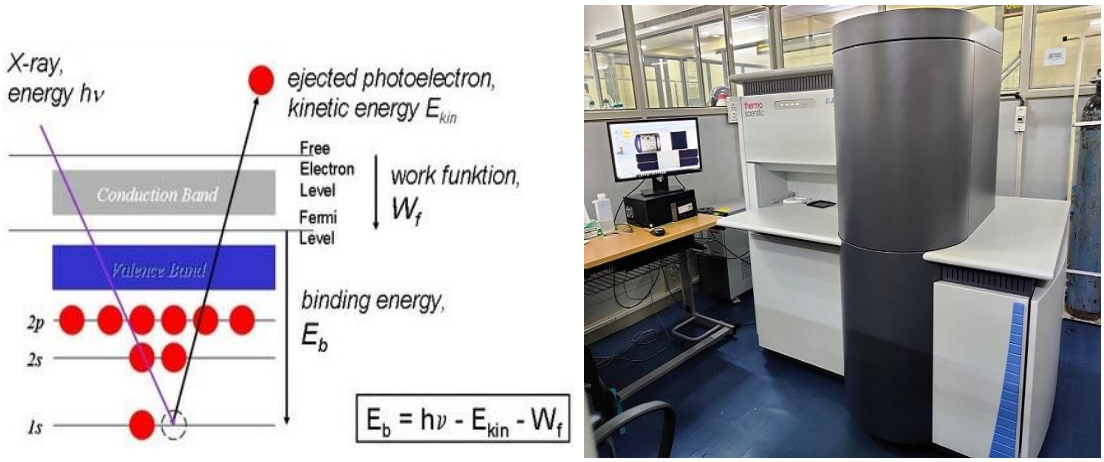


**Figure 2.7:** Working principal and experimental set up for XPS spectroscopy.

In this technique, very high energy X-ray falls on the surface of the sample placed in an ultra-high vacuum ($10^{-8}$-$10^{-9}$ millibars) condition and interacts with core level electrons

of the atoms at the surface. An incident photon directly transfers its energy to the core level electron and ejects the electron out of the surface which is collected by the electron energy analyser detector. Electron energy analyser detects the photo ejected electrons and provides an energy spectrum of binding energy. Analysis of the Intensity (electron counts) versus binding energy curve identifies the elements with Z=3 and above, present in the sample and their oxidation states. This technique is applied for almost all kind of samples like ceramics, glasses, alloys, polymers, semiconductors etc.

### 2.3.5 Impedance Spectroscopy

Impedance spectroscopy is a non-destructive technique which can measure dielectric and charge transport properties of electro-ceramic materials. With the help of this technique, the electrical behaviour, impedance, ac or dc conductivity can be determined. Numerous electrical responses such as impedance, dielectric constant, dielectric loss etc. were recorded as a function of frequency and temperature by using an impedance analyser (KEYSIGHT-E4990A) shown in **Fig. 2.8**. The measurements were done in air atmosphere in the frequency range 20Hz to 10MHz from room temperature to 600°C. Complex impedance measurement directly provide details about ac resistance, parallel or series capacitance, dielectric permittivity, dielectric loss etc. which are further processed to explain many interesting properties like-relaxation phenomena, the ion dynamics correlating the structure and electrical property of the material. In this thesis work, calcined powder samples were made into cylindrical pellets by uniaxial pressing (up to 60 MPa) in a 12 mm diameter stainless steel die with the help of hydraulic press. As a binder, 2% PVA (Polyvinyl Alcohol) solution in water were used for preparation of pellets of all the samples. Electroding of the pellets were done by applying fired-on silver (cured at 500 $^{o}$C) paste on both flat sides of the pellet.

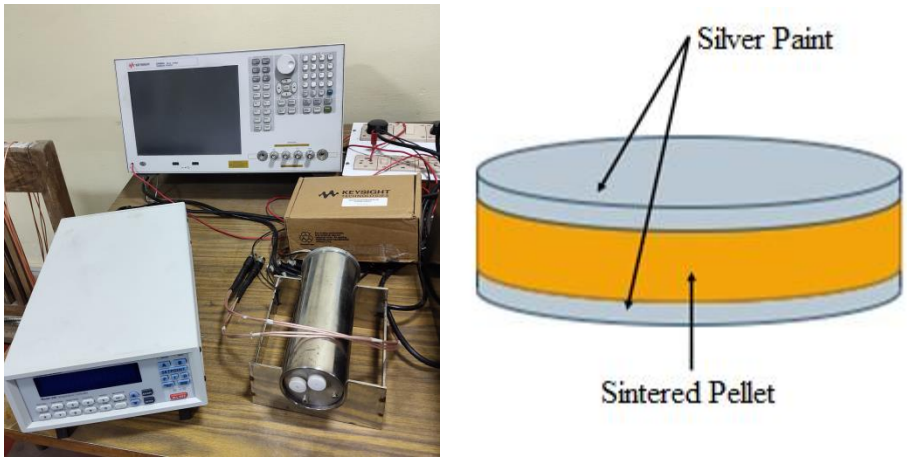


**Figure 2.8:** Set up of Impedance Analyser and schematic diagram of an electroded pellet.

The silver electrode pellet behaves like a parellel plate capicitor filled with a diectric material as shown in **Fig. 2.8**. These pellets were mounted on a sample holder inside a tubular furnace and ac-signal of various frequencies were applied using two probe method. The electrical responses were recorded up to 600°C in heating run, at 20 different frequencies varying across 20 Hz to 10 MHz by KEYSIGHT-E4990A. A thermocouple is used in the furnace for sensing the temperature. The measurement was fully interfaced with the computer for automatic data recording.

### 2.3.5.1 Permittivity Calculation

The impedance analyzer provides temperature and frequency dependent capacitance ($C_p$) values of the electroded pellets which behave like a parallel plate capacitor. Silver coated circular flat surfaces behave as parallel plates and the space between them is filled with dielectric material. Relative permittivity (dielectric constant) can be calculated with the help of following formula-

$$\varepsilon_r = \frac{C_p d}{\varepsilon_0 A} \qquad (2.3)$$

Where Cp denotes the capacitance of parallel plate capacitor (pellet), d is the thickness of the pellet, A is the area of the parallel face of the pellet and $\varepsilon_0$ is the permittivity of the vacuum. Using this formula, permittivity values at various temperatures is estimated. Analysis of the temperature dependent permittivity curve illustrates the high and low temperature phase stability and dielectric relaxations of the investigated samples.

### 2.3.5.2 Conductivity estimation from Nyquist plot

The complex impedance technique measures the ac-responses and can provide the details of electrical properties of the material including the contribution of the microstructural entities such as grain, grain boundary and interfacial contribution across a wide range of frequency and temperature. AC electrical information can be analysed in any of the four fundamental formalisms which are interconnected to one another by the following formulas-

$$\text{Complex admittance:} \quad Y^* = Y' + iY''$$

$$\text{Complex impendence:} \quad Z^* = (Y^*)^{-1} = Z' - iZ''$$

$$\text{Complex modulus:} \quad M^* = M' + iM'' = i\omega C_0 Z^*$$

$$\text{Complex permittivity:} \quad \varepsilon^* = (M^*)^{-1} = \varepsilon' - i\varepsilon'' = (i\omega C_0 Z^*)^{-1}$$

Here, $\omega_0 = 2\pi f$, is angular frequency and $C_0 = {}^{\varepsilon_o A}/_{d}$ is the vacuum capacitance.

Sometimes, it is difficult to describe the data whether the electrical response e.g. geometrical capacitance is due to long range (conductivity) or short range (dipole relaxation) property of the material. The imaginary part of the impedance (Z'') and conductance (Y'') are reasonable when long-range property is predominant whereas ε'' and M'' are used for analysis when localized relaxation dominates [122]. The correlation

between microstructure and conductivity can be deduced from the analysis of the real and imaginary part of the impedance (complex impedance analysis). An impedance plot in complex plane i.e. plot of the real part of complex impedance (Z') along x-axis against imaginary part of complex impedance (Z'') along y-axis are known as Cole-Cole or Nyquist plot as shown in **Fig. 2.9**. Nyquist representation gives a quick idea of qualitative understanding about resistance and hence conductivity of the sample at a particular temperature. Typically, in polycrystalline materials, Nyquist plot contains a progression of half circles, ascribing relaxation phenomena with various time constants corresponding to the presence of grain (bulk), grain boundary and electrode-interface charge carrier relaxations. The semi-circular arc in the low frequency region corresponds to contribution of electrode-material interface, semi-circular arc in the intermediate frequency region to grain boundary and semi-circular arc in the high-frequency region is attributed to the bulk response of the material, as illustrated in **Fig. 2.9**. Sum of intercepts of all the semicircles on the real axis gives the total resistance (R) of the material. Hence conductivity of the material can be determined by using the following formula

$$\sigma = \frac{L}{SR} \qquad (2.4)$$

Where L denotes thickness and S denotes circular cross-sectional area of the sample. Fitting of Nyquist plots were done using ZSIMP-WIN version 2 software with appropriate equivalent circuit. The equivalent circuit model should have three parallel RC circuits connected in series corresponding to relaxation of each of grain, grain boundary and electrode interface.

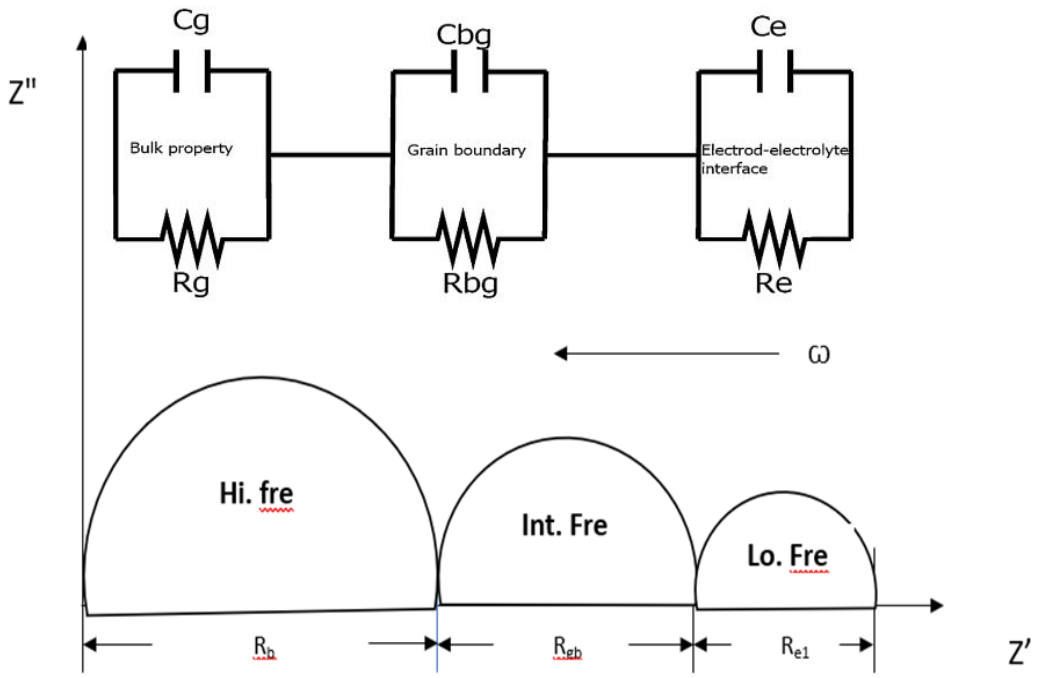


**Figure 2.9:** Typical Nyquist plot having semi-circular arcs with intercepts on the real axis giving rise to the corresponding resistances such as Bulk, Grain Boundary and electrode-interface resistances respectively.

### 2.3.6 Ultraviolet-visible (UV-Vis) spectroscopy Characterization

UV-Vis spectroscopy is one of the basic and very useful analytical tool for absorption or reflectance spectroscopy in the UV-visible spectral region. The absorbance data, obtained as function of wavelength by UV-Vis spectrophotometer, can be used to estimate the band gap of the material. In this thesis, SHIMADZU UV-2600; UV-Vis spectrophotometer was used to record the optical absorption spectrum as shown in **Fig. 2.10,** along with the schematic diagram of its working principle. A spectrophotometer consists of a light source, a monochromator (diffraction grating), sample holders and a photodiode with photomultiplier tube as detector. A diffraction grating separates the different wavelengths to make them monochromatic. Tungsten filament (300-2500 nm) and $D_2$ arc (deuterium) lamp (190-400 nm) are used as continuous source of ultraviolet region and LEDs and Xenon Arc Lamps are taken for

the visible range radiation. UV-Vis spectrophotometer is useful for polycrystalline powder as well as for liquid samples. The schematic diagram for the mechanism of the UV-Vis spectrophotometer is shown in the **Fig. 2.10.** It compares the intensity of light passed through a sample ($I$) to the intensity of light passing through reference ($I_o$). The ratio $I/I_o$ expressed as percentage by the following formula are referred as % transmittance (%T)

$$\% \, T = \frac{I}{I_0} \times 100 \qquad (2.5)$$

Absorbance can be calculated from percentage transmittance using the following equation:

$$A = - \log (T/100) \qquad (2.6)$$

Similarly, the reflectance (R or %R) of the sample can also be determined. In this case, the intensity of light reflected from a sample is compared with the intensity of light reflected from a reference material. Generally, UV-Vis spectroscopy of solid-state materials is performed in Reflectance mode which is converted into absorbance with the help of Kubelka Munk function. The optical band gap is estimated using the well-known Tauc equation given by the following equation (J. Tauc. 1968).

$$(\alpha h\nu)^n = A(h\nu - E_g) \qquad (2.7)$$

where α, h, ν, 'A' and $E_g$ are absorbance, Planck constant, frequency of photon, band tailoring constant and band gap energy respectively and 'n' denotes the nature of transition n= 2 for direct allowed band gap and n = ½ for indirect allowed band gap.

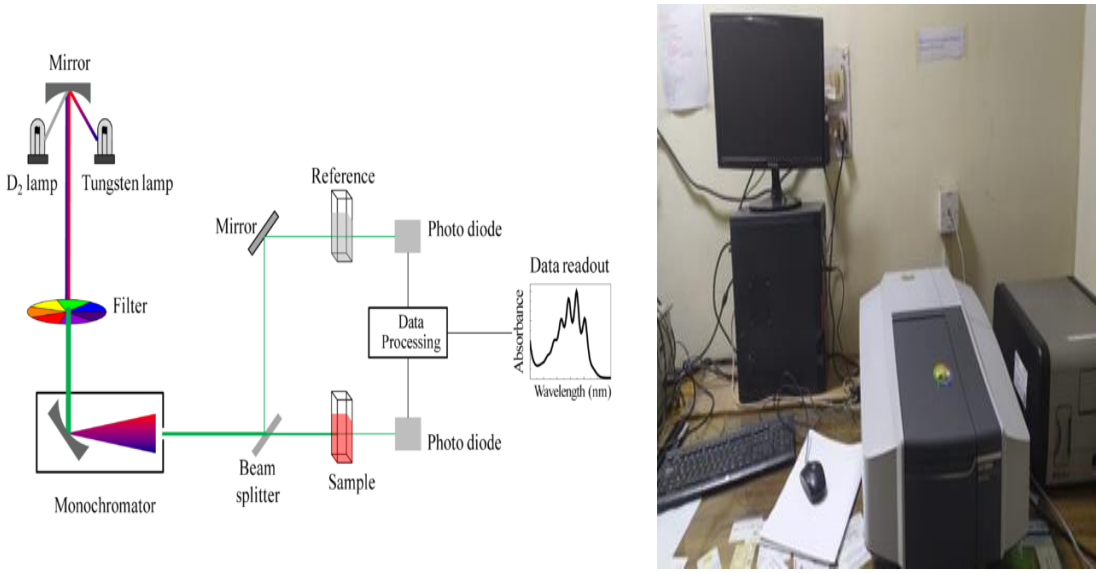


**Figure 2.10:** Schematic diagram for set up of UV-Vis spectroscopy.

### 2.3.7 Ferroelectric Characterization

Ferroelectric property is one of the basic properties required for the ferroelectric photovoltaic materials. Polarization (P)-Electric Field (E) hysteresis loop were recorded to check the ferroelectric behaviour of the materials. In this work, hysteresis loops were traced with the help of Radiant Precision Premier II ferroelectric tester from Radiant Technologies, USA using the Sawyer-Tower circuit as depicted in the **Fig. 2.11**. An outline of the instrumentation for the P-E loop measurement technique is shown in the **Fig. 2.12**. High voltage amplifier, Function generator, Current to voltage converter, displacement measurement system etc. are the key components of the P-E loop measurement set up. 'Displacement measurement system' makes this set up able to measure the Strain- Electric field (S-E) hysteresis loops too. From P-E loop measurement, we can determine the remanent polarization, saturation polarization, Coercive field, electrical storage density, efficiency etc. of the material. In this thesis, the hysteresis loops were measured at room temperature and with varying frequency range of 1 Hz to 1 kHz with a sinusoidal ac- signal.

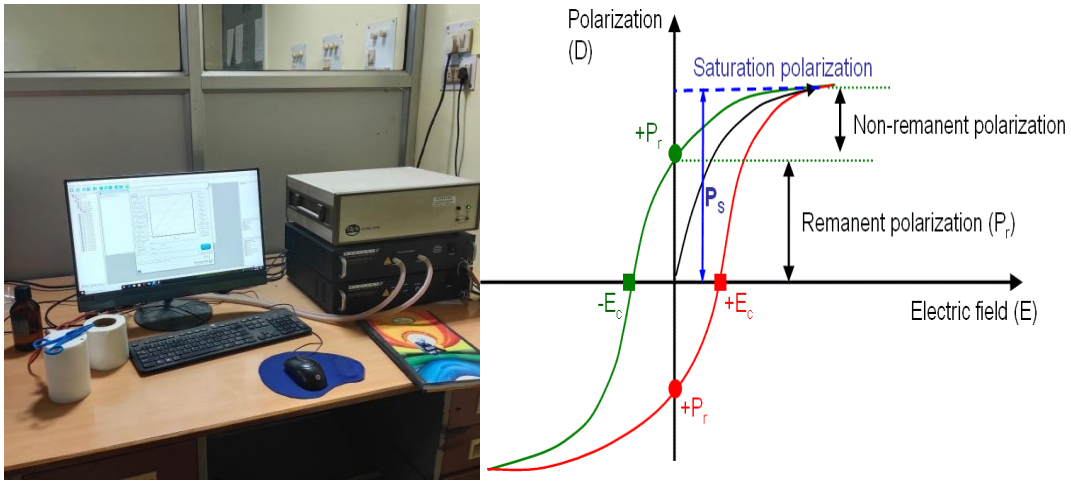


**Figure 2.11:** Hysteresis loop and the Radiant Precision Premier II ferroelectric tester for P-E loop measurement.

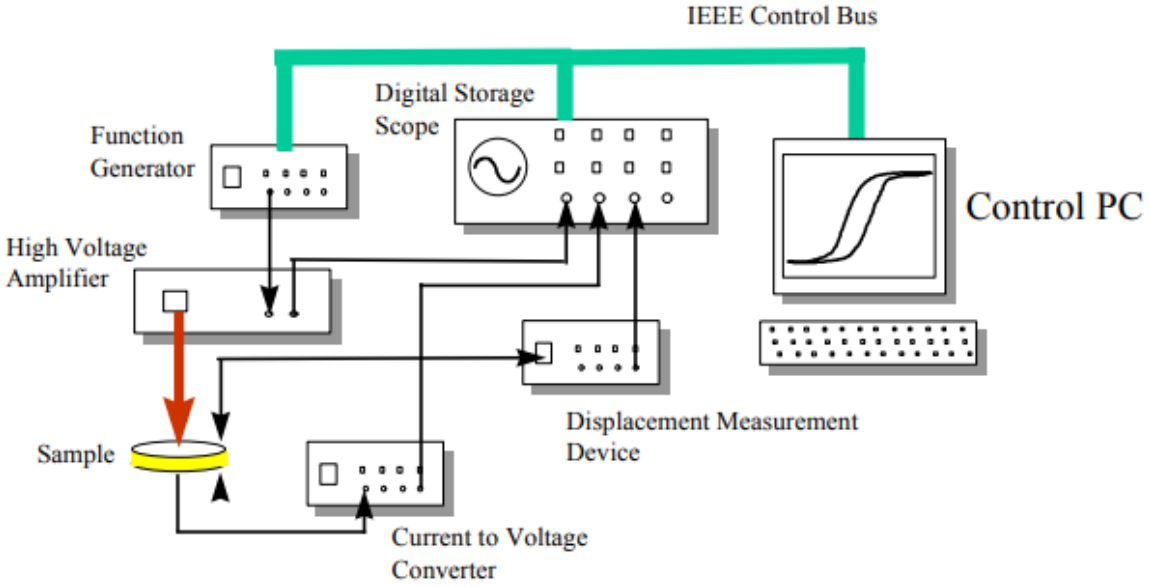


**Figure 2.12:** Schematic building block for set up of P-E loop measurement.

## 2.4 Conclusions

This chapter briefly describes synthesis method for sample preparation and each of the characterization techniques adopted in this thesis. We have used solid state synthesis method using ball milling, one of the most facile synthesis methods for the preparation of all the samples. Different characterizations and property analysis softwares to analyse and interpret the result data, as well as with their theoretical aspects

are also described. The subsequent chapters will discuss the results of investigation on various ferroelectric photovoltaic materials.